Hindawi
Heteroatom Chemistry
Volume 2019, Article ID 3507837, 10 pages
https://doi.org/10.1155/2019/3507837

Research Article

Computational Studies of 4-Formylpyridinethiosemicarbazone and Structural and Biological Studies of Its Ni(II) and Cu(II) Complexes

Mydhili P. Sripathi,[1] Sireesha Berely,[1] and Chittireddy Venkata Ramana Reddy[2]

[1]*Department of Chemistry, Nizam College, Osmania University, Hyderabad, India*
[2]*Department of Chemistry, Jawaharlal Nehru Technological University Hyderabad, Hyderabad, India*

Correspondence should be addressed to Chittireddy Venkata Ramana Reddy; vrr9@yahoo.com

Received 30 October 2018; Accepted 30 January 2019; Published 3 March 2019

Academic Editor: David Barker

To understand the stability, chelation behaviour, and biological activity of 4-Formylpyridinethiosemicarbazone (H4FPT), it is important to recognize its interactive geometry. Hence, computational studies on geometrically optimized structures of thione and thiol forms of H4FPT were performed. Binary metal complexes of the ligand, H4FPT (L) with the Ni(II) and Cu(II) metal ions (M), were synthesized and characterized by various spectroanalytical techniques as elemental analysis, molar conductance, magnetic susceptibility measurements, LC-MS, TGA, IR, UV-Visible, ESR, and powder XRD. Elemental analysis, LC-MS, and TGA studies indicate 1:2 (ML_2) composition for mononuclear Ni(II) complex and 1:1 (ML) composition for dinuclear Cu(II) complex. Electronic absorption titrations, fluorescence quenching studies, and viscosity measurements suggest intercalative mode of binding of the complexes with calf thymus DNA (CT-DNA). These complexes also promote hydrolytic cleavage of plasmid pBR322. The ligand (H4FPT) and its complexes showed moderate-to-good activity against Gram-positive and Gram-negative bacterial strains. The DPPH radical scavenging studies showed antioxidant nature of both complexes.

1. Introduction

Cancer is a growing cause of death of human beings worldwide, which necessitated the search for new therapeutic agents. The coordination complexes either as drug or as prodrug can be used as potential anticancer agents. These complexes involve specific interactions with the DNA, leading to the destruction of the cancer cells [1]. The discovery of cis-platin laid foundation to metal-based drugs in chemotherapy [2]. However, use of cis-platin and its next-generation drugs like carboplatin and oxaplatin is limited owing to their side effects or acquired drug resistance. This has led to the development of few other metal ion complexes as Bi(II), Ru(II), Ru(III),Cu(II), Re(I), and so forth with potential anticancer activity [3].

Transition metal complexes of thiosemicarbazones are of much interest due to their broad spectrum of pharmacological activity such as antitumor, antiviral, and antibacterial activities [4–7]. Based on the nature of metal ions, thiosemicarbazones behave as bidentate or tridentate ligands and bind in either anionic or neutral forms [8]. Pyridine-2-carboxaldehydethiosemicarbazone was first among the α-(N)-thiosemicarbazones reported to be carcinostatic [9, 10].

In order to understand the origin of the biological activity of any molecule, it is essential to identify how the molecule interacts with the active site in biological systems and preferable orientation for its interaction. Therefore, it is important to recognize interactive geometry of the molecule and estimate its contribution towards attractive interactions with the active site of the target. Computational chemistry generates data that complements experimental data on the structure, properties, and reactions of substances. Energy parameters such as single point energy and heat of formation give an idea about stability of molecule, while HOMO-LUMO energy gap indicates the ease of the compounds to enter into the reactions [11, 12]. QSAR properties that are generated by computation provide an insight into chemical properties, which govern the biological activity, and in tu rn

drug-like action of the molecules, before being synthesized [13].

Besides our earlier studies on the N-substituted 4-formylpyridine thiosemicarbazone complexes [14], the present communication reports computational studies such as energy parameters, FMO analysis and QSAR properties of the ligand, 4-Formylpyridinethiosemicarbazone (H4FPT, L) and synthesis, characterization, DNA binding, cleavage, and antibacterial and antioxidant studies of its Ni(II) and Cu(II) complexes.

2. Materials and Methods

All the chemicals used were of reagent grade and were obtained from Sigma-Aldrich. Semiempirical quantum chemical calculations were carried out by HyperChem 7.5 Molecular Modeling program. LC-MS of the ligand and its complexes were recorded on LCMS 2010A, Shimadzu spectrometer; elemental analysis was done on Thermo Finnigan 1112 elemental analyzer. Molar conductivity was measured using Digisun-909 digital conductivity meter. Magnetic susceptibilities were measured at room temperature on Faraday balance-7550. Thermogravimetric analysis of the complexes was carried out on TG balance, TA: Q/50 in the temperature range of 0 to 1000°C with a ramp of 20°C per min. The IR spectra in KBr were recorded on Shimadzu Prestige-21 FTIR spectrometer. ^{1}H-NMR (with D_2O exchange) and ^{13}C-NMR were recorded on Varian 400 MHz NMR spectrometer and UV spectra in DMSO were recorded on Shimadzu UV 2450 spectrophotometer. ESR spectrum of copper complex was obtained from Jeol, JES–FA 200 ESR spectrometer. Powder XRD were recorded on a SMART Bruker D8 Focus X-ray diffractometer using Cu KR X-radiation (λ = 1.5406 Å) at 40kV and 30mA. Diffraction patterns were collected over 2θ range of 5–80° at a step size of 0.089° and with a step time of one second and Match! Software (Crystal Impact) was used for phase identification. Fluorescence spectra were recorded on RF-5301-PC Shimadzu spectrofluorimeter and Ostwald's viscometer was used for viscosity measurement studies.

2.1. Computational Studies. To understand the stability and reactivity of the ligand, H4FPT quantum mechanical and molecular mechanical calculations were made using Hyperchem 7.5 by semiemperical (PM3) method.

2.2. Synthesis of 4-Formylpyridinethiosemicarbazone, H4FPT (L). The ligand, H4FPT, was synthesized by known procedure [4]. To the hot aqueous solution of thiosemicarbazide (0.456g, 5 mmol), 4-formylpyridine (0.47 mL, 5 mmol) was added and stirred for 1 h at room temperature. Product formation was monitored by TLC in 1:3 ethyl acetate and petroleum ether as mobile phase. The resultant solid product was filtered, washed thoroughly with water, dried, and recrystallized from 1:1 ethanol-water.

Characterization data for H4FPT: Cream solid; Yield 85%, m.p. 228-230°C.

IR (KBr, υ, cm^{-1}): 827(C=S), 991(N-N), 1598(C=N), 3151(N-H, hydrazine), 3261, 3419 (N-H, thioamide). ^{1}H NMR, (δ, ppm): 7.7 (d, 2H, aromatic H, J = 4.4 Hz), 8.5 (d, 2H, aromatic H, J = 4.4 Hz), 7.9 (s, 1H, H-C=N), 8.2 (s, 1H, N-CS-NH, D_2O exchangeable), 8.4 (s, 1H, N-CS-NH, D_2O exchangeable), 11.6 (s, 1H, N-N-H, D_2O exchangeable). ^{13}C NMR (δ, ppm): 141.8, 121.5, 139.9, 150.4, 178.9. UV-Visible, (λ_{max}, nm): 331, 252. C H N analysis, $C_7H_8N_4S$, Found, %: C 46.82; H 4.58; N 30.91. Calculated, %: C 46.6; H 4.43; N 31.06. APCI-MS (+): m/z 181 $[M+1]^+$, 121 $[C_6H_6N_3]^+$, 78 $[C_5H_4N]^+$, 61 $[CSNH_2]^+$.

2.3. Synthesis of Metal Complexes. To the hot ligand solution (0.50 g, 2.7mmol in 35 mL CH_3OH), aqueous solution of $CuCl_2$ (0.1815 g, 1.35 mmol in 5 mL)/$NiCl_2.6H_2O$ (0.321 g, 1.35 mmol in 5 mL) was added and refluxed for 5 to 8 h. The pH of the solution was adjusted by addition of few drops of methanolic ammonium hydroxide. The resultant solid complexes were filtered, washed with hot methanol to remove unreacted ligand and with water to remove unreacted metal ion, followed by petroleum ether, and dried in vacuum [14, 15].

Characterization data for Ni(II) Complex: Yellow solid, m.p. > 300°C.

IR (KBr, υ, cm^{-1}): 815(C=S), 1012 (N-N), 1568, 1603(C=N), 3146(N-H, hydrazine), 3293, 3423 (N-H, thioamide). UV-Visible (λ_{max}, nm): 885, 445, 390. C H N analysis, Found, %: C 34.25; H 3.7; N 22.61. Calculated, %: C 34.25; H 3.59; N 22.83. APCI-MS: m/z 473 $[M+2]^+$.

Characterization data for Cu(II) Complex: Brown solid, m.p. > 300°C.

IR (KBr, υ, cm^{-1}): 819 (C=S), 1014 (N-N), 1597 (C=N), 3142 (N-H, hydrazine), 3236, 3313 (N-H, thioamide). UV-Visible (λ_{max}, nm): 993, 728, 412. C H N analysis, Found, %: C 24.41; H 3.51: N 16.80. Calculated, %: C 24.57; H 3.21; N 16.38. ESI-MS: m/z 684 $[M+1]^+$.

2.4. DNA Binding Studies

2.4.1. Electronic Absorption Titrations. The concentration of CT-DNA solution prepared in 5 mM Tris HCl -50 mM NaCl, pH 7.2 buffer was calculated as 153 μM from its UV absorbance at 260 nm (ε = 6600 M^{-1} cm^{-1}) [14, 16]. Stock solutions of the complexes in DMSO were diluted to 20 μM using Tris HCl buffer. Absorption titrations were carried out with increasing amounts of CT-DNA from 0 to 210 μL. Samples were equilibrated for ten minutes before each scan. The CT-DNA solution was added to both the test and reference solutions to eliminate the absorption by CT-DNA.

2.4.2. Fluorescence Quenching Studies. Fluorescence quenching studies were carried out in Tris HCl buffer with 20 μM DNA and 20 μM EB wherein [DNA] / [EB] = 1. Stock solutions of the complexes in DMSO were diluted to 50 μM using Tris HCl buffer. Fluorescence quenching titrations were carried out with increasing amounts of complexes from 0 to 400 μL. Emission spectra were recorded at excitation wavelength of 520 nm and emission wavelength between 530 and 770 nm [17].

2.4.3. Viscosity Studies. Relative viscosity studies were carried out using an Ostwald's viscometer immersed in thermostatic

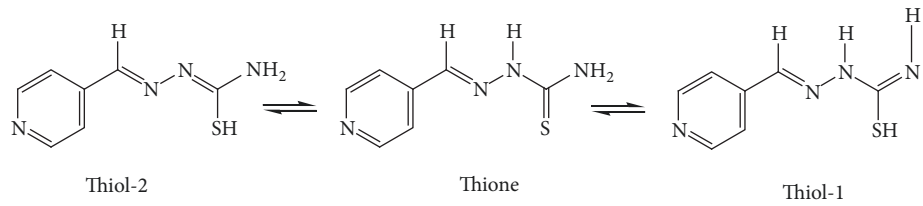

Figure 1: Thione and thiol forms of the H4FPT.

water bath at 27°C. Stock solutions of the complexes were prepared in DMSO and diluted to 50 μM with Tris HCl buffer. Increasing amounts of the complexes (0-100 μL) were added to 10 mL of the Tris HCl buffer and 100 μL of 200 μM CT-DNA solutions taken in viscometer. The flow time was measured with a digital stopwatch. Each sample was measured thrice and an average flow time was considered [18].

2.5. DNA Cleavage Studies. The pBR322 plasmid DNA dissolved in TE buffer (10 mM Tris-HCl (pH 7.5), 1 mM EDTA) containing 0.1% sodium azide and TAE buffer (pH 8.0; 40 mM Tris base, 20 mM acetic acid, and 1 mM Na_2EDTA) was used for gel electrophoresis. 3 μL of super coiled pBR322 DNA (100ng/μL) was added to 15, 30, and 45 μM complexes and incubated for 1h at 37°C. Later, 1 μL of 0.25% bromophenol blue (loading buffer) was added and loaded onto 0.8% agarose gel. The electrophoresis was carried at 60 V for 2 h until bromophenol blue had moved through 75% of the gel. Later, the gel was stained with EB and then destained in sterile distilled water. The plasmid bands were visualized under transilluminator and photographed [19].

2.6. Antibacterial Studies. In vitro antibacterial activity of the synthesized compounds was investigated by disc diffusion method [19] against Gram-positive bacteria, *Staphylococcus aureus* and *Bacillus subtilis*, and Gram-negative bacteria, *Escherichia coli* and *Klebsiella pneumoniae*. Sterile nutrient agar plates were seeded with pure test culture using spread plate technique. Sterile discs of 5 mm in diameter impregnated with 5 μL of sample solutions were placed at equidistance. Discs containing DMSO without any test compounds served as a control, which have no activity. Gentamicin was used as standard. Zone of inhibition in mm was recorded after 24 h of incubation at 37°C. Each assay was triplicated and results were averaged [20].

2.7. Antioxidant Studies. The antioxidant activity of Ni(II) and Cu(II) complexes was determined by using 2,2-diphenyl-1-picrylhydrazyl (DPPH) assay [21, 22]. Stock solutions of the complexes were prepared by dissolving 2mg of the samples in 6 mL of DMSO. Various amounts of the test compounds (50, 100, 150, 200, and 250 μg/mL) from the stock solutions were diluted to 2 mL with methanol. To these solutions, 1.0 mL of 0.4 mM methanol solution of DPPH was added and stirred vigorously. Test solutions were incubated for 30 minutes at room temperature in dark. The antioxidant activity is measured in terms of decrease in absorbance (UV-VIS Shimadzu) of DPPH at 517nm. DPPH solution without sample was used as control and ascorbic acid was used as reference [21–23].

Table 1: Molecular properties of H4FPT.

Property	Thione	Thiol-1	Thiol-2
Single point energy (K Cal/mole)	-2021.88	-2036.92	-2028.04
Heat of Formation (K Cal/mole)	109.54	94.51	103.38
Dipole Moment (Debye)	7.41	4.24	3.68

3. Results and Discussion

3.1. Computational Studies of 4-Formylpyridinethiosemicarbazone (H4FPT). As H4FPT exhibits thione-thiol tautomerism (Figure 1), both forms were built and their geometry optimization is performed using molecular mechanics with uniform force field (UFF).

From the energies listed in Table 1, it is evident that both forms are stable. Close proximity of heat of formation suggests their possible coexistence. Calculated dipole moment values indicate more polar nature of thione form.

3.1.1. Frontier Molecular Orbital (FMO) Analysis. Highest occupied molecular orbital (HOMO) of a molecule with high energy has a tendency to donate electrons to appropriate acceptor molecule with low energy and lowest unoccupied molecular orbital (LUMO). An electronic system with a large HOMO-LUMO gap should be less reactive than a system with small gap. The hardness (η) corresponds to the gap between the HOMO and LUMO orbital energies. The larger the HOMO-LUMO energy gap is, the more hardness ((η) = ($E_{HOMO} - E_{LUMO}$)/2) of the molecule will be. The hardness, in turn, is associated with the stability of the chemical system [11, 12]. In the present study, the HOMO-LUMO gap (Table 2) is sufficiently large, indicating that the H4FPT is a stable molecule. However, thiol-1 and thiol-2 forms have high η values compared to thione form, indicating more stability over thione form as also supported by their ionization energy and electron affinity values listed in Table 2.

The optimized geometries of thione and thiol forms of H4FPT and its electrostatic potential, electron density mappings, and the molecular orbital surfaces have been generated (Figure S1). Negative electrostatic potential around nitrogen atoms in pyridine ring, imine, and thioamide moieties and thione sulphur indicate the regions of high electron density

Table 2: FMO analysis of H4FPT.

Energy	Thione	Thiol-1	Thiol-2
E_{HOMO} (ev)	-8.803	-8.943	-9.097
E_{LUMO} (ev)	-1.137	-1.063	-0.798
$E_{HOMO} - E_{LUMO}$ (ev)	7.666	7.88	8.299
Hardness (η)	3.833	3.94	4.149
I.E = $-E_{HOMO}$	8.803	8.943	9.097
EA = $-E_{LUMO}$	1.137	1.063	0.797

Table 3: QSAR properties of H4FPT.

Property	Thione	Thiol-1	Thiol-2
Partial Charge	0.0e	0.0e	0.0e
Surface area (Approx) $Å^2$	313.38	330.96	309.74
Surface area (grid) $Å^2$	370.10	372.26	371.42
Volume $Å^3$	562.26	566.17	562.75
Hydration Energy (K Cal/mole)	-16.81	-18.48	-15.12
log P	2.01	2.31	2.47
Refractivity $Å^3$	52.14	50.80	50.68
Polarizability $Å^3$	20.28	19.61	19.61
Mass (amu)	180.23	180.23	180.23

and are more susceptible to electrophilic attack [23]. This suggests that these atoms in H4FPT are potential donor sites and can coordinate to metal(II) ions to form complexes.

3.1.2. Quantitative Structure-Activity Relationship (QSAR) Properties. QSAR studies help to recognize and compute the physicochemical properties of a drug and its effect on biological activity. Highly polarizable molecules can strongly attract other molecules and can also increase aqueous solubility. Molar refractivity is the volume occupied either by an individual atom or by a group of atoms. As per Lorentz-Lorenz relationship [13], polarizability and the molar refractivity enhance with the volume and the molecular weight. Due to these properties, molecule can interact with the receptor and show biological activity.

Hydrophobic character supports the molecule to bind the receptors and activates it as an agonist, which can be measured in terms of partition coefficient (log P). From the plot of log P versus log(1/Conc), it is possible to correlate the drug with biological activity. In general, drugs with log P ≈ 3.0 have higher chance of being absorbed, > 4.0 require lipid formulations, and < 2.0 show both hydrophilic and hydrophobic characters and will be difficult to formulate [24, 25].

The log P value obtained from these studies listed in Table 3 is less than 3, which indicates that the H4FPT can cross the cell membrane and establish binding interactions with the target site. Thus, the molecule exhibits pharmacological or biological activity.

3.2. Characterization of Metal Complexes. The Ni(II) and Cu(II) complexes are coloured, microcrystalline, stable to air and moisture, and soluble in methanol, ethanol, acetone, DMSO, and DMF. Elemental analysis data, mass spectra, and TGA revealed the formation of Ni(II) complex with 1:2 (M:L) composition and Cu(II) complex with 1:1 (M:L) composition. Low molar conductivity (0-6 Scm^2M^{-1}) of the complexes indicates their nonelectrolytic nature [26]. Presence of chloride ion in the complexes was established from Volhard's test [27].

3.2.1. Liquid Chromatograms. Both metal complexes showed single peak with the retention time in the range of 0.550 to 0.656 min, indicating their purity.

3.2.2. Mass Spectra. In APCI (+) MS of Ni(II) complex (Figure S2b), the peaks have been observed at m/z 473 $[M+2]^+$ and at m/z 454 due to loss of one coordinated water molecule. Loss of coordinated chloride ion is indicated by a peak at m/z 420 and this peak also indicates 1:2 metal to ligand ratio.

In the ESI (+) MS of Cu(II) complex (Figure S2c), $[M+1]^+$ peak has been observed at m/z 684. Peaks at m/z 666 and 629 may be due to loss of lattice and coordinated water molecules, respectively. Peak at m/z 487 corresponds to 2L:2M of the complex. A small peak at m/z 128 reveals the dimeric nature of the metal ion.

3.2.3. Thermogravimetric Analysis. Thermogram of Ni(II) complex (Figure S3a) showed desolvation up to 80°C followed by decomposition in four steps. In the first step, the weight loss of 3.9% (230-280°C) can be assigned to loss of one mole of coordinated water molecule. In the second step, the weight loss of 31.5% at 280°C corresponds to the loss of chloride ion and $CSNH_2$ moiety, followed by two-step decomposition between 320 and 500°C (15.03%) and between 500 and 791°C (17.22%) indicating the decomposition of the complex moiety. The residue (18.38%) at 791°C reveals the metal ion percentage corresponding to 1:2 (M:L) composition of the complex.

In the thermogram of Cu(II) complex (Figure S3b), the desolvation has been observed up to 80°C, followed by the decomposition in four steps. Loss of one lattice water molecule (2.5%) and two coordinated water molecules (5.2%) was evident from the weight loss at 80 to 160°C and 160 to 220°C, respectively. A steep curve (38% weight loss) in the range of 220 to 400°C followed by gradual weight loss (13.62%) till 940°C indicates loss of coordinated chloride ions. Later, the decomposition of the complex can be observed with 35.24% of final residue, which indicates metal oxide corresponding to 1:1 (M:L) composition of Cu(II) complex.

3.2.4. IR Spectra. IR spectra of both complexes (Figures S4b and S4c) showed broad peaks in the range of 3050-3325 cm^{-1} indicating the presence of water molecules. In the IR spectrum of Ni(II) complex (Table 4), shift in νC=N and νC=S towards lower frequency as compared to that of the ligand spectrum (Figure S4a) shows coordination of azomethine nitrogen and sulphur atoms with the metal ions [28, 29]. The presence of both νN-H and a new νC=N in the complex spectrum reveals that both the thione and thiol forms of ligand are coordinated with the Ni(II) metal ion in the complex.

The IR spectrum of Cu(II) complex (Table 4) showed that both the C=N and C=S stretching bands have been shifted

Table 4: IR spectral data of H4FPT and complexes.

Compound	υ(N-H)	υ(C=N)	υ(C=S)
H4FPT (L)	3151	1598	827
Ni(II) complex	3146	1603, 1568	815
Cu(II) complex	3142	1597	819

towards lower frequency, suggesting azomethine nitrogen and thiol sulphur to be potential coordination sites [30, 31].

In the far IR region of the spectra of the complexes, the υ(M-N), υ(M-S), υ(M-Cl), and υ(M-OH_2) bands have been observed. In the IR spectrum of Cu(II) complex, the peaks at 320 and 285 cm^{-1} give an evidence for terminal and bridging M-Cl bonds, respectively. Analysis of IR spectral data indicates that the ligand is bidentate with azomethine nitrogen and thione/thiol sulphur as potential donor sites forming five membered chelates with the metal ions.

3.2.5. UV-Visible Spectra. In the electronic spectrum of Ni(II) complex (Figure S5b), three d-d transitions at 885 nm [υ_1, $^3A_{2g} \longrightarrow {}^3T_{2g}$ (F)], 445 nm [υ_2, $^3A_{2g} \longrightarrow {}^3T_{1g}$ (F)], and 390 nm [υ_3, $^3A_{2g} \longrightarrow {}^3T_{1g}$ (P)] which indicate distorted octahedral geometry of the complex are observed [32].

The electronic spectrum of Cu(II) complex (Figure S5c) showed three absorption bands at 993 nm [υ_1, $^2B_{1g} \longrightarrow {}^2A_{1g}$], 728 nm [$\upsilon_2$, $^2B_{1g} \longrightarrow {}^2B_{2g}$], and 412 nm [$\upsilon_3$, $^2B_{1g} \longrightarrow {}^2E_{1g}$]. These transitions indicate the distorted octahedral geometry, due to Jahn-Teller distortion [15].

3.2.6. ESR Spectrum. The ESR spectrum of Cu(II) complex (Figure S6) in DMSO showed peaks corresponding to $g^{\parallel}$ 2.166 and $g^{\perp}$ 2.041. The greater values of $g^{\parallel}$ suggest distortion from regular octahedral geometry with $^2B_{1g}$ ground state and anisotropic environment around copper ion. $g^{\parallel} < 2.3$ indicates covalent nature of the Cu-L bond. Both $g^{\parallel} > g^{\perp} > 2.0023$ indicate the presence of unpaired electron in d_{x2-y2} orbital of the Cu(II) ion. Axial symmetry parameter, $G < 4$, is due to exchange interaction between metal centers of polycrystalline compound [9].

3.2.7. Magnetic Susceptibility Measurements. The magnetic moment value (2.72 BM) measured for the Ni(II) complex corresponds to two unpaired electrons, indicating outer orbital complex with distorted octahedral geometry. The magnetic susceptibility measurements for the Cu(II) complex showed diamagnetic nature, while the same complex showed ESR activity. This may be due to antiparallel alignment of the electronic spin of the unpaired electron (d^9) present on the adjacent Cu(II) ions in dinuclear complex, as also known from mass spectrum of the complex.

3.2.8. Powder X-Ray Diffraction Studies. Match! Software (Crystal Impact) is used for phase identification of the ligand and Ni(II) and Cu(II) complexes (Figures S7a, S7b, and S7c) and found to be appreciably matching with the reference patterns [33]. The XRD pattern of complexes differs from the ligand. Many feeble peaks have been observed in the complex diffractograms indicating their microcrystalline nature. Size of the crystallite was calculated from Debye Scherrer's equation [34, 35],

$$D = \frac{0.9\lambda}{\beta \cos\theta} \quad (1)$$

where D is crystallite size; λ is the wavelength of X-ray diffraction; β is the full width at half maximum (FWHM) of observed peaks; θ is the angle of diffraction. The average crystallite sizes for H4FPT and Ni(II) and Cu(II) complexes were 0.28, 0.25, and 0.76 nm, respectively. From the matched phases, the crystal system can be proposed to be orthorhombic for ligand and monoclinic for both complexes.

From the analysis of various spectroanalytical data, the proposed structures for Ni(II) and Cu(II) complexes are presented in Figure 2.

3.3. DNA Binding Studies

3.3.1. Electronic Absorption Titrations. Electronic absorption spectroscopy is extensively used to study the binding interactions between metal complexes and CT-DNA. Intercalation of metal complex into CT-DNA leads to hypochromism as the aromatic chromophore of the complex establishes strong $\pi \longrightarrow \pi*$ interactions with the base pairs [14, 36]. In this study, both Ni(II) and Cu(II) complexes showed hypochromic shift as shown in Figure 3, indicating their intercalation into CT-DNA, resulting in conformational change of CT-DNA.

From the titration data, intrinsic binding constant, K_b, has been calculated from the equation

$$\frac{[DNA]}{(\varepsilon_a - \varepsilon_f)} = \frac{[DNA]}{(\varepsilon_b - \varepsilon_f)} + \frac{1}{K_b(\varepsilon_b - \varepsilon_f)} \quad (2)$$

where [DNA] is the concentration of CT-DNA in base pairs; ε_a, ε_b, and ε_f are the extinction coefficients of apparent, bound, and free complex, respectively. Ratio of slope to intercept from the plot of [DNA] versus [DNA]/($\varepsilon_a - \varepsilon_f$) gives K_b of the complex. The calculated intrinsic binding constants, K_b, for Ni(II) and Cu(II) complexes are 3.0×10^4 M^{-1} and 1.25×10^4 M^{-1}, respectively, indicating their binding affinity towards CT-DNA.

Free energy of DNA-complex system can be calculated using the following equation:

$$\Delta G = -RT \ln K_b \quad (3)$$

where ΔG is Gibb's free energy in kJ mol^{-1}, R is the gas constant (8.314 $JK^{-1}mol^{-1}$), T is the temperature in Kelvin, and K_b is the intrinsic binding constant of DNA-complex [36].

Free energy (ΔG) is a measure of the spontaneity of binding the complex to DNA. The calculated ΔG for Ni(II) and Cu(II) complexes, − 26.41 and − 24.16 $kJmol^{-1}$, respectively, indicate that Ni(II) complex binds to the CT-DNA more spontaneously than Cu(II) complex..

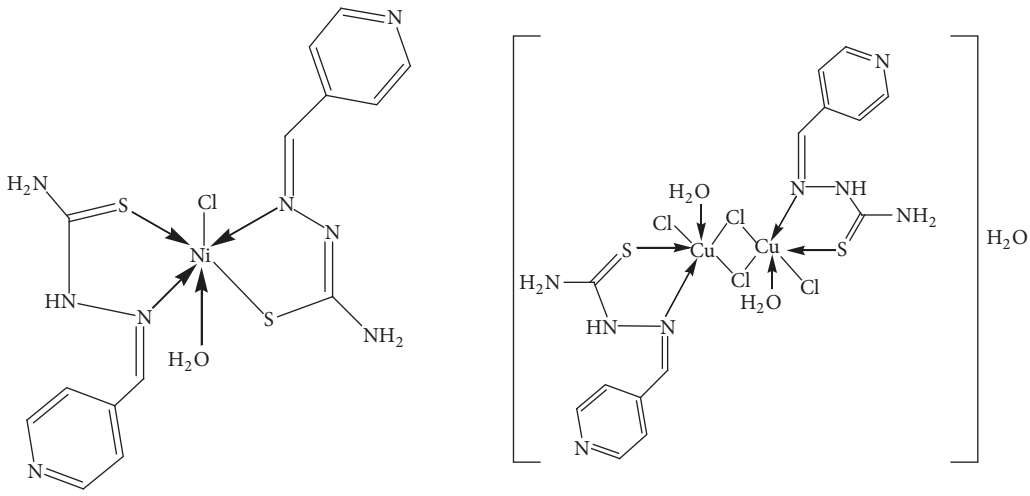

Figure 2: Proposed structures of Ni(II) and Cu(II) complexes.

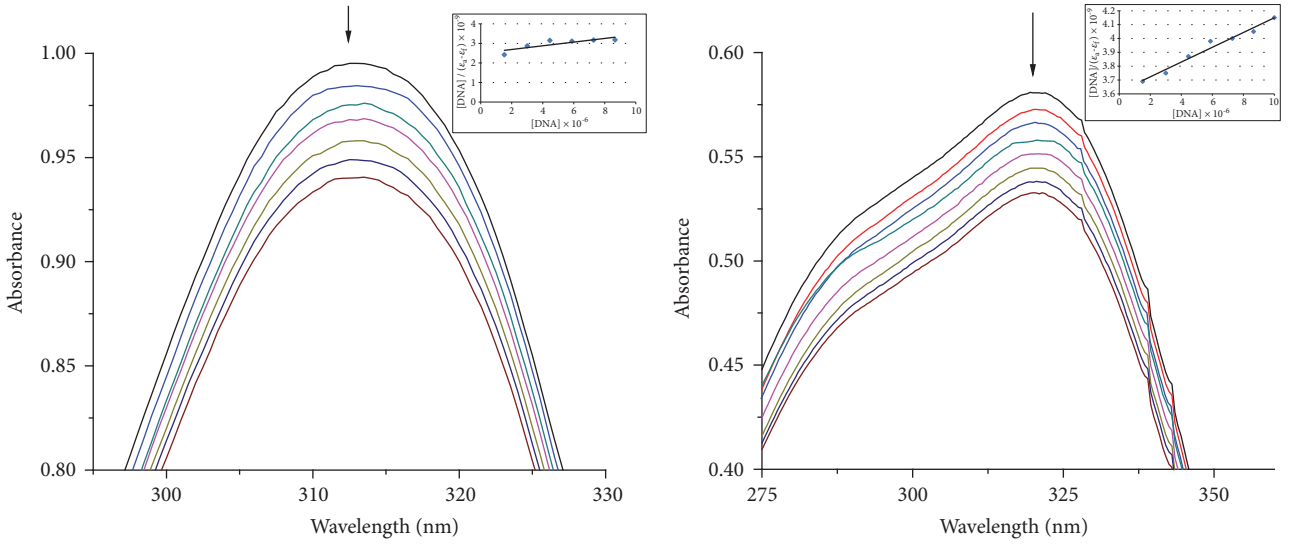

(a) Ni(II) complex (b) Cu(II) complex

Figure 3: Absorption spectra of Ni(II) and Cu(II) complexes [20μM] in increasing amounts (0-210μL) of CT-DNA, [DNA]=153μM [inset: plots of [DNA] versus [DNA] / ($\varepsilon_a - \varepsilon_f$)].

3.3.2. Fluorescence Quenching Studies. To study the mode of binding between CT-DNA and metal complex, competitive binding experiment was performed. Ethidium bromide (EB) is a conjugate planar molecule and has very weak fluorescence emission intensity, which enhances considerably on its intercalation between the base pairs of DNA, which results in DNA-EB complex. When the metal complex is introduced into the solution, the metal complex molecules displace EB from DNA-EB and the fluorescence emission intensity of DNA-EB complex will be quenched. Fluorescent emission of EB (20 μM) bound to CT-DNA (20 μM) in the absence and in the presence of metal complex is shown in Figure 4. The quenching of emission intensity at 611 nm of the DNA-EB with increase in metal complex concentration suggests the intercalation of complex with CT-DNA [17].

The linear Stern-Volmer quenching constant, K_{sv}, was obtained from classical Stern-Volmer equation:

$$\frac{I_0}{I} = 1 + K_{sv} r \quad (4)$$

where I_0 and I are the fluorescence intensities in the absence and presence of the quencher and r is the ratio of the total concentration of the complex to that of CT-DNA. The K_{sv} values have also been obtained from the plot I_0/I vs r. The quenching curves were in accordance with linear Stern–Volmer equation [17], which indicates that the metal complexes are bound to CT-DNA. From the linear plot of I_0/I versus r, the K_{sv} values for the complexes were found to be 0.092 and 0.090, respectively, which suggest the DNA binding strength of Ni(II) complex > Cu(II) complex.

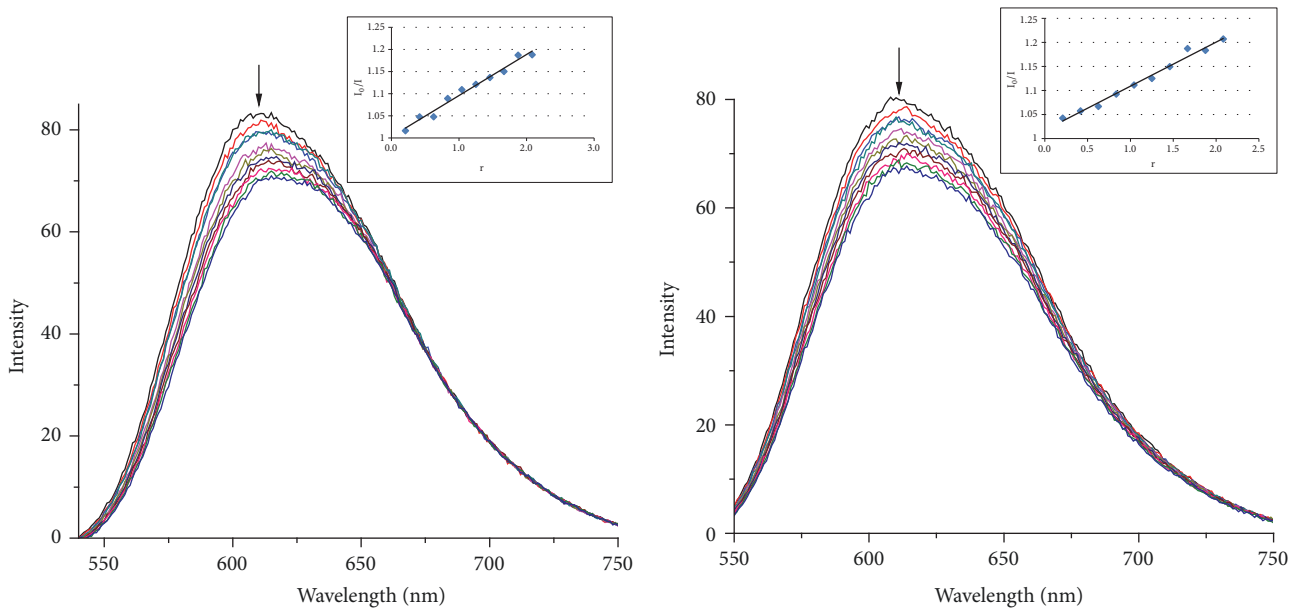

(a) Ni(II) complex (b) Cu(II) complex

FIGURE 4: Emission spectra of EB–DNA, with increasing amounts (0-400μL) of Ni(II) and Cu(II) complexes, [complex]=50μM, [DNA]=20μM (inset: Stern–Volmer quenching curves).

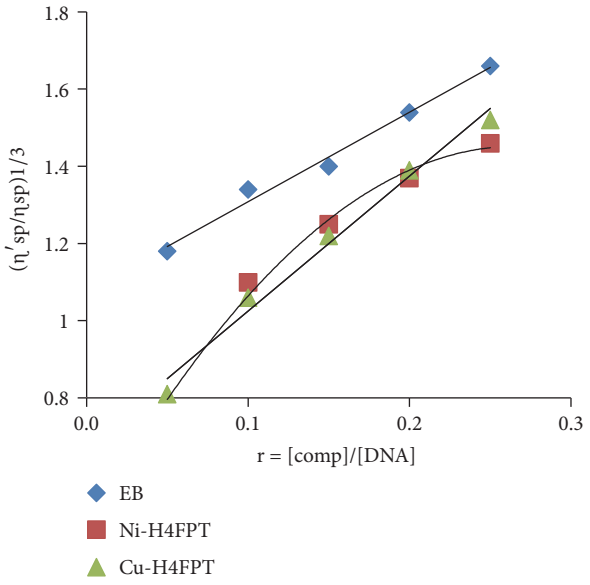

FIGURE 5: Effect of increasing amount of EB and Ni(II) and Cu(II) complexes on the relative viscosity of CT-DNA at 27.0°C.

3.3.3. Viscosity Studies. Though binding strength between metal complex and CT-DNA can be studied by spectroscopic methods, they may not give adequate information about binding mode. Hydrodynamic measurements like viscosity of metal complex bound DNA in solution can give useful information in the absence of crystallographic data. An intercalation can lengthen the DNA helix, as its base pairs get separated to accommodate the binding complex, which in turn increases the viscosity of DNA. A partial intercalation of complex could bend or kink the DNA helix leading to decrease in helical length of DNA. If the complex interacts with DNA through electrostatic interaction or by groove binding, the relative viscosity is not affected [18].

Data were presented as $(\eta'_{sp} / \eta_{sp})^{1/3}$ versus ratio of the concentration of the compound to CT-DNA (r), where η'_{sp} is the viscosity of CT-DNA in the presence of the complex and η_{sp} is the viscosity of CT-DNA in the absence of the complex [18]. In the present study, both metal complexes showed an increase in viscosity due to their intercalation into CT-DNA as shown in Figure 5.

3.4. DNA Cleavage Studies. Super coiled (SC) plasmid DNA has a cyclic super coiled double strand structure. To activate the phosphodiester links for nucleophilic attack, the metal ions in the complexes serve as Lewis acids and metal coordinated water molecules act as nucleophiles. On electrophoresis, the intact SC plasmid DNA migrates faster. When SC form is cleaved due to the action of the complex, it gets converted to nicked coiled (NC) form, which moves slowly. Cleavage of both strands leads to linear form, which migrates between SC and NC forms, as the shorter molecules move easily through the pores of the gel [19]. The results are presented in Figure 6, which indicate that both complexes promote hydrolytic cleavage of plasmid pBR322 DNA, due to scission in SC forms to NC forms (lanes 2 to 7). With the increase in concentration of the complexes, the intensity of NC band increases, indicating the concentration dependency of nuclease activity.

3.5. Antibacterial Studies. Antibacterial activities of H4FPT and its complexes have been tested on the Gram-positive bacteria, *Staphylococcus aureus* and *Bacillus subtilis*, and Gram-negative ones, *Escherichia coli* and *Klebsiella pneumoniae*.

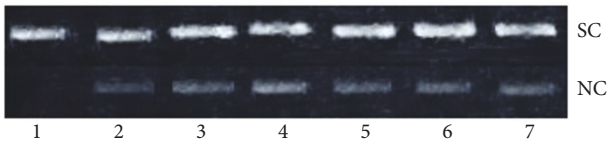

Figure 6: Changes in the agarose gel electrophoresis pattern of pBR322 plasmid DNA through hydrolytic cleavage: (1) DNA alone; (2, 3, 4) DNA + Cu(II) complex (15, 30, and 45 μM); (5, 6, 7) DNA + Ni(II) complex (15, 30, and 45 μM).

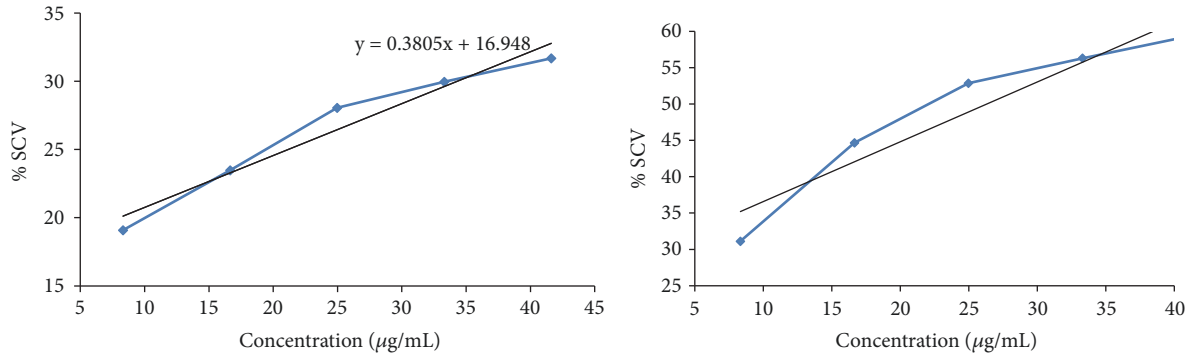

(a) Ni(II) complex (b) Cu(II) complex

Figure 7: DPPH scavenging activity of Ni(II) and Cu(II) complexes.

Table 5: Antibacterial activity of H4FPT and its complexes.

S. No.	Compound	Zone of inhibition (mm)			
		S. aureus	*B. subtilis*	*E. coli*	*K. pneumoniae*
1	H4FPT (L)	6	7	----	----
2	Ni(II) complex	6	8	----	----
3	Cu(II) complex	11	10	13	14

The results are listed in Table 5. The ligand and its Ni(II) complex were found to inhibit the growth of only Gram-positive bacteria under study. The Cu(II) complex was active against both the Gram-positive and Gram-negative bacteria (Figure S8). This may be due to the lipophilic nature of the complexes, which favours their permeability into bacterial cell membranes and inhibits the growth of the bacteria [20].

3.6. Antioxidant Studies. Antioxidants react with DPPH radical and reduce it to DPPH-H and as a consequence the absorbance decreases. DPPH is a stable free radical with purple colour that turns yellow when scavenged. The degree of discoloration and decrease in absorbance (UV-VIS) indicate the scavenging potential of the compounds in terms of hydrogen donating ability. The scavenging reaction between DPPH and an antioxidant (HD) can be written as

$$(\text{DPPH}) + (\text{H-D}) \longrightarrow \text{DPPH-H} + (\text{D}) \quad (5)$$

The percentage of DPPH radical scavenging activity (% SCV) was calculated by using the following equation:

$$\%\ \text{DPPH scavenging ability (\% SCV)} = \frac{A_c - A_s}{A_c} \times 100 \quad (6)$$

where A_c and A_s are absorbance values of control and the sample, respectively.

The IC_{50} values obtained from plots of concentration of the sample versus % SCV give the concentration of the sample that leads to reduction of 50% in the free radical concentration [21, 22]. In the present study, the IC_{50} values were observed as 86.53 μg/mL (61.1 μM) for Ni(II) complex and 26.31 μg/mL (12.84 μM) for Cu(II) complex, respectively. This indicates that the Cu(II) complex exhibits better antioxidation activity than Ni(II) complex (Figure 7).

4. Conclusions

Computational studies of H4FPT revealed the nitrogen atoms in pyridine ring, imine, and thioamide linkages and thione sulphur as potential sites for electrophilic attack and can coordinate with the metal ions to form complexes. QSAR properties generated for the ligand in its both forms indicate its ability to act as drug. The H4FPT acts as bidentate ligand and forms chelates with the metal ions. The Ni(II) complex is mononuclear with 1:2 (ML_2) composition and Cu(II) complex is dinuclear with 1:1 (M:L) ratio. The DNA binding studies revealed that both complexes intercalate into the base pairs of the CT-DNA and cleave the super coiled form of plasmid pBR322 DNA to nicked form. The ligand and the metal complexes can inhibit the growth of bacteria under study. Both complexes have shown antioxidant activity, of which the Cu (II) complex showed better activity.

Data Availability

The data/figures pertaining to spectral characterization, computational analysis, thermograms, powder X-ray, and

biological evaluation to support the findings of this study are included within the supplementary information file.

Conflicts of Interest

The authors declare that there are no conflicts of interest regarding the publication of this paper.

Acknowledgments

The authors acknowledge Osmania University, JNT University Hyderabad, and School of Chemistry, University of Hyderabad, for providing research facilities to carry out this work.

Supplementary Materials

Molecular graphs of the ligand (H4FPT) and spectra of the ligand and its Ni(II) and Cu(II) complexes are incorporated as supplementary material mentioned as Figures S1–S7. Agar plates showing antibacterial activity of H4FPT (L) and its Ni(II) and Cu(II) complexes with zone of inhibition are presented in Figure S8. The fluorescence emission data of DNA binding studies of the complexes are listed in Tables S1 and S2. *(Supplementary Materials)*

References

[1] M. Frezza, S. Hindo, D. Chen et al., "Novel metals and metal complexes as platforms for cancer therapy," *Current Pharmaceutical Design*, vol. 16, no. 16, pp. 1813–1825, 2010.

[2] U. Ndagi, N. Mhlongo, and M. E. Soliman, "Metal complexes in cancer therapy - an update from drug design perspective," *Drug Design, Development and Therapy*, vol. 11, pp. 599–616, 2017.

[3] M. P. M. Marques, "Platinum and palladium polyamine complexes as anticancer agents: the structural factor," *ISRN Spectroscopy*, vol. 2013, Article ID 287353, 29 pages, 2013.

[4] S. Chandra, M. Tyagi, and M. S. Refat, "Spectroscopic, thermal and antibacterial studies of Mn(II) and Co(II) complexes derived from thiosemicarbazone," *Journal of the Serbian Chemical Society*, vol. 74, no. 8-9, pp. 907–915, 2009.

[5] A. R. Cowley, J. R. Dilworth, P. S. Donnelly, and J. Woollard-Shore, "Synthesis and characterisation of new homoleptic rhenium thiosemicarbazone complexes," *Dalton Transactions*, no. 4, pp. 748–754, 2003.

[6] I. C. Mendes, L. R. Teixeira, R. Lima, H. Beraldo, N. L. Speziali, and D. X. West, "Structural and spectral studies of thiosemicarbazones derived from 3- and 4-formylpyridine and 3- and 4-acetylpyridine," *Journal of Molecular Structure*, vol. 559, no. 1-3, pp. 355–360, 2001.

[7] S. A. Elsayed, A. M. El-Hendawy, S. I. Mostafa, and I. S. Butler, "Transition metal complexes of 2-formylpyridinethiosemicarbazone (HFpyTSC) and X-ray crystal structures of $[Pd(FpyTSC)(PPh_3)]PF_6$ and[Pd(FpyTSC)(SCN)]," *Inorganica Chimica Acta*, vol. 363, no. 11, pp. 2526–2532, 2010.

[8] E. Bermejo, A. Castiñeiras, I. García, and D. X. West, "Spectral and structural studies of mercury(II) complexes of 2-pyridineformamide N(4)-dimethylthiosemicarbazone," *Polyhedron*, vol. 22, no. 8, pp. 1147–1154, 2003.

[9] P. F. Rapheal, E. Manoj, and M. R. Prathapachandra Kurup, "Copper(II) complexes of N(4)-substituted thiosemicarbazones derived from pyridine-2-carbaldehyde: Crystal structure of a binuclear complex," *Polyhedron*, vol. 26, no. 4, pp. 818–828, 2007.

[10] D. K. Demertzi, J. R. Miller, N. Kourkoumelis, S. K. Hadjikakou, and M. A. Demertzis, "Palladium(II) and platinum(II) complexes of pyridine-2-carbaldehyde thiosemicarbazone with potential biological activity. Synthesis, structure and spectral properties. Extended network via hydrogen bond linkages of [Pd(PyTsc)Cl]," *Polyhedron*, vol. 18, no. 7, pp. 1005–1013, 1999.

[11] S. Rajeev, D. Kumar, S. Bhoop, V. Singh, and K. R. Sharma, "Molecular structure, vibrational spectroscopic and HOMO, LUMO studies of S-2-picolyl-β-N-(2-acetylpyrrole) dithiocarbazate schiff base by quantum chemical investigations," *Research Journal of Chemical Sciences*, vol. 3, pp. 79–84, 2013.

[12] R. Singh, D. Kumar, Y. C. Goswami, and R. Sharma, "Synthesis, spectral studies and quantum-chemical investigations on S-benzyl β-N-(4-NN biscynodiethylaminophenylmethylene)dithiocarbazate," *Arabian Journal of Chemistry*, 2014.

[13] Z. Almi, S. Belaidi, T. Lanez, and N. Tchouar, "Structure activity relationships, QSAR modeling and drug-like calculations of TP inhibition of 1,3,4-oxadiazoline-2-thione derivatives," *International Letters of Chemistry, Physics and Astronomy*, vol. 37, pp. 113–124, 2014.

[14] S. P. Mydhili, B. Sireesha, and Ch. Venkata Ramana Reddy, "Synthesis, DNA binding, cleavage and antibacterial studies of nickel (ii) and copper (II) complexes of 4-formylpyridine N (4)-methylthiosemicarbazone," *Journal of Chemical and Pharmaceutical Research*, vol. 8, pp. 78–85, 2016.

[15] S. Chandra, S. Raizada, M. Tyagi, and P. K. Sharma, "Spectroscopic and biological approach of Ni(II) and Cu(II) complexes of 2-pyridinecarboxaldehyde thiosemicarbazone," *Spectrochimica Acta Part A: Molecular and Biomolecular Spectroscopy*, vol. 69, no. 3, pp. 816–821, 2008.

[16] H. Wu, T. Sun, K. Li et al., "Synthesis, crystal structure, and DNA-binding studies of a nickel(II) complex with the bis(2-benzimidazolymethyl)amine ligand," *Bioinorganic Chemistry and Applications*, vol. 2012, Article ID 609796, 7 pages, 2012.

[17] C.-Y. Zhou, J. Zhao, Y.-B. Wu, C.-X. Yin, and Y. Pin, "Synthesis, characterization and studies on DNA-binding of a new Cu(II) complex with N^1,N^8-bis(l-methyl-4-nitropyrrole-2-carbonyl)triethylenetetramine," *Journal of Inorganic Biochemistry*, vol. 101, no. 1, pp. 10–18, 2007.

[18] T. Topala, A. Bodoki, L. Oprean, and R. Oprean, "Experimental techniques employed in the study of metal complexes-DNA-interactions," *Farmacia*, pp. 1049–1061, 2014.

[19] P. R. Reddy and A. Shilpa, "Interaction of DNA with small molecules: role of copper histidyl peptide complexes in DNA binding and hydrolytic cleavage," *Indian Journal of Chemistry - Section A Inorganic, Physical, Theoretical and Analytical Chemistry*, vol. 49, no. 8, pp. 1003–1015, 2010.

[20] S. Chandra, S. Parmar, and Y. Kumar, "Synthesis, spectroscopic, and antimicrobial studies on bivalent zinc and mercury complexes of 2-formylpyridine thiosemicarbazone," *Bioinorganic Chemistry and Applications*, vol. 2009, Article ID 851316, 6 pages, 2009.

[21] D. Ashok, E. V. L. Madhuri, M. Sarasija et al., "Synthesis, biological evaluation and molecular docking of spirofurochromanone derivatives as anti-inflammatory and antioxidant agents," *RSC Advances*, vol. 7, no. 41, pp. 25710–25724, 2017.

[22] I. P. Ejidike and P. A. Ajibade, "Synthesis, characterization and biological studies of metal(II) complexes of (3E)-3-[(2-{(E)-[1-2,4-Dihydroxyphenyl)ethylidene]amino}ethyl)imino]-1phenylbutan-1-ones schiff base," *Molecules*, vol. 20, no. 6, pp. 9788–9802, 2015.

[23] C. Cojocaru, A. Rotaru, V. Harabagiu, and L. Sacarescu, "Molecular structure and electronic properties of pyridylindolizine derivative containing phenyl and phenacyl groups: comparison between semi-empirical calculations and experimental studies," *Journal of Molecular Structure*, vol. 1034, pp. 162–172, 2013.

[24] G. Patrick, *An Introduction to Medicinal Chemistry*, Oxford University Press, Oxford, UK, 5th edition, 2013.

[25] T. Hou, J. Wang, W. Zhang, W. Wang, and X. Xu, "Recent advances in computational prediction of drug absorption and permeability in drug discovery," *Current Medicinal Chemistry*, vol. 13, no. 22, pp. 2653–2667, 2006.

[26] R. Aman, G. Matela, C. Sharma, and S. Chaudhary, "Biologically active diorganotin(IV) complexes of N-(2-hydroxy-3-isopropyl-6-methyl benzyl) glycine," *Arabian Journal of Chemistry*, vol. 8, no. 5, pp. 698–705, 2015.

[27] G. Svelha, *Vogel's Text Book of Qualitative Inorganic Analysis*, Pearson Education, India, 7th edition, 2009.

[28] R. L. De Lima, L. R. De Souza Teixeira, T. M. Gomes Carneiro, and H. Beraldo, "Nickel(II), Copper(I) and Copper(II) complexes of bidentate heterocyclic thiosemicarbazones," *Journal of the Brazilian Chemical Society*, vol. 10, no. 3, pp. 184–188, 1999.

[29] H. Beraldo, R. Lima, L. R. Teixeira, A. A. Moura, and D. X. West, "Crystal structures and IR, NMR and UV spectra of 4-formyl- and 4-acetylpyridine *N*(4)-methyl- and *N*(4)-ethylthiosemicarbazones," *Journal of Molecular Structure*, vol. 559, no. 1-3, pp. 99–106, 2001.

[30] G. Kanagaraj and G. N. Rao, "Synthesis and characterization of complexes of cobalt(II), nickel(II), zinc(II), cadmium(II) and mercury(II) with p-acetamidobenzaldehyde thiosemicarbazone," *Polyhedron*, vol. 12, pp. 383–387, 1993.

[31] D. X. West, H. Beraldo, and A. A. Nassar, "Nickel(II) complexes of 4-acetamidobenzaldehyde N(4)-substituted thiosemicarbazones," *Transition Metal Chemistry*, vol. 24, no. 1, pp. 25–28, 1999.

[32] A. B. P. Lever, *Inorganic Electronic Spectroscopy*, Elsevier Science Publishers, Amsterdam, 2nd edition, 1984.

[33] MATCH! Version 2.x, Crystal Impact, H.Putz & K.Brandenburg GbR, Kreuzherrenstr. 102, 53227 Bonn, Germany.

[34] P. E. Ikechukwu and A. A. Peter, "Synthesis, characterization, antioxidant, and antibacterial studies of some metal(II) complexes of tetradentate schiff base ligand: (4E)-4-[(2-(E)-[1-(2,4-dihydroxyphenyl)ethylidene]aminoethyl)imino]pentan-2-one," *Bioinorganic Chemistry and Applications*, vol. 2015, Article ID 890734, 9 pages, 2015.

[35] W. Bembee Devi and R. K. B. Singh, "Syntheses, characterization and spectroscopic studies on schiff base complexes of diaminomaleonitrile," *International Journal of Science and Research*, vol. 2, pp. 312–318, 2013.

[36] K. Karami, Z. Shirani-Sarmazeh, M. Hosseini-Kharat, J. Lipkowski, and M. Saeidifar, "Synthesis, spectral characterization, crystal structure and in vitro DNA/protein binding studies of phosphorous ylide palladacyclic complexes containing azide group," *Journal of Photochemistry and Photobiology B: Biology*, vol. 144, pp. 11–19, 2015.